

Comparison of Sound Insulation Performance of Water Drop and Trapezoidal Sound Barriers

Arif DOĞAN¹ , Ahmet ASLANDAĞ² , Paşa YAYLA¹ 

¹ Marmara University, Engineering Faculty, Mechanical Engineering Department, 34840, Istanbul, Türkiye

² Kasso Mühendislik San. ve Tic. A.Ş., 34953, Istanbul, Türkiye

Abstract

With increasing urbanization and industrialization, noise pollution has become a significant environmental issue. This study compares the sound insulation performance of two different sound barrier designs: water drop and trapezoidal. COMSOL Multiphysics software for computational simulations is used to calculate sound transmission loss (STL). The results indicated that the water drop design provides more effective sound insulation compared to the trapezoidal model. Additionally, economic analyses suggest that the water drop design may offer long-term advantages despite higher initial costs.

Keywords: Sound insulation, Water drop design, Trapezoidal design, Noise barrier, COMSOL Multiphysics, Sound transmission loss, STL.

I. INTRODUCTION

Noise pollution is an escalating issue in urban areas, significantly affecting the quality of life for residents. As cities grow denser, the challenge of mitigating environmental noise becomes increasingly complex. Traditional methods of noise reduction, such as using sound barriers, have proven effective but are not without limitations. These barriers, typically constructed from materials like glass and plastic composites, face issues related to durability and effectiveness under various conditions.

In this study, the comparative performance of two innovative noise barrier designs: a trapezoidal model and a water drop-shaped model is investigated. The primary goal is to determine which design offers superior sound insulation and overall efficiency. One of the advanced simulation tools, such as COMSOL Multiphysics, is used to conduct detailed analyses.

The trapezoidal design is well-known for its ease of production and cost-effectiveness. In contrast, the water drop design, with its aesthetically pleasing shape, promises better performance in sound insulation but at a higher production cost. This study aims to provide a comprehensive analysis of these designs, considering both their sound insulation performance and practical application in real-world scenarios.

By integrating numerical simulations and empirical data, this study seeks to advance the current understanding of noise barrier technologies. The findings will help in developing more effective and durable noise mitigation solutions for urban environments, ultimately contributing to improved living conditions and public health.

The trapezoidal sound barrier design is popular due to its ease of production and cost-effectiveness. However, there is potential that the more intricate droplet (water drop) design could offer superior visual aesthetics and sound insulation. This study aims to compare the two designs in terms of sound insulation performance. By evaluating these factors, the study seeks to determine if the droplet model can serve as a viable and advantageous alternative to the conventional trapezoidal system, addressing a gap in current noise barrier design exploration.

1.2. Literature Review

The literature mainly focuses on three main subtopics relevant to sound barriers. Firstly, sound barriers play a crucial role in addressing noise pollution by providing practical solutions to mitigate excessive environmental noise. This subtopic provides an overview of the fundamental principles governing sound barriers and their essential function in noise mitigation [1, 2]. By reducing the intensity of unwanted noise, sound barriers significantly enhance the quality of life in urban and suburban environments [3, 4]. Secondly, with the rise of urbanization and industrialization, noise pollution has become a pervasive challenge, prompting the development of effective countermeasures such as sound barriers [5, 6]. These barriers are designed to impede the transmission of sound waves from noise sources, evolving from basic physical structures to advanced solutions that consider effectiveness, aesthetics, and environmental factors [7, 8]. The historical evolution and modern advancements in sound barrier technology are explored, highlighting their primary role in reducing environmental noise and improving community well-being [9, 10]. Thirdly, understanding the mechanisms employed by sound barriers is crucial for grasping their functional significance in noise mitigation [11, 12]. These mechanisms include absorption, where materials dissipate sound energy as heat; reflection, where sound waves are redirected back toward the source; and diffraction, where sound waves bend around or over the barrier [13, 14]. Additionally, sound barriers aim to achieve transmission loss by preventing sound energy from passing through and may incorporate resonance control and vibration-damping materials to minimize structure-borne noise [15, 16]. Modern advancements also include adaptive technologies that adjust to changing conditions, optimizing noise reduction in real-time [17].

1.2.1. Trapezoidal sound barriers: Design, performance, and applications

Trapezoidal sound barriers are a specialized category of noise mitigation structures, distinguished by their unique trapezoidal shape, as seen in Figure 1. This design features a tapered appearance, with one side of the barrier being notably shorter than the opposite side, resulting in a distinctive trapezoid-like silhouette [7, 9]. This particular configuration is not only aesthetically pleasing but also optimized to enhance the barrier's effectiveness in deflecting and absorbing sound. Consequently, trapezoidal sound [18, 19] barriers are a significant choice for various noise control applications.



Figure 1. Trapezoidal prototype view, actual view, cad view.

1.2.2. Droplet model for sound barriers: Aesthetic and acoustic advancements

The Droplet Model for sound barriers represents a groundbreaking integration of aesthetic appeal and acoustic innovation, as seen in Figure 2. Inspired by the natural form and characteristics of droplets, this model aims to elevate noise control solutions by advanced sound attenuation capabilities [20, 21]. It is designed to not only mitigate noise effectively but also to enhance the visual landscape, offering a harmonious blend of functionality and design [22, 23].

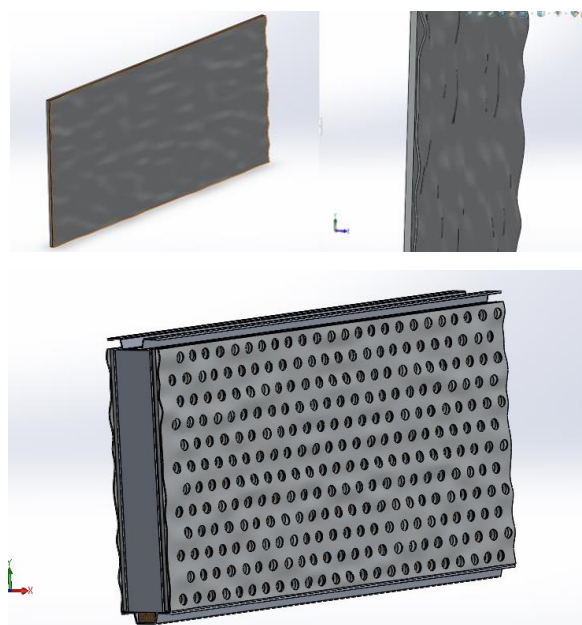


Figure 1. Water-drop design CAD view.

II. MATERIALS AND METHODS

This section describes the materials and methodologies employed in comparing the sound insulation performance of the trapezoidal and water drop sound barrier designs. The study utilized computational simulations to analyze Sound Transmission Loss (STL) across these different geometries, ensuring a comprehensive evaluation of their effectiveness.

2.1. Materials

The materials used for the sound barriers in this study include:

Aluminum Panels: Both designs were constructed using aluminum due to their favorable properties such as durability, lightweight, and ease of fabrication.

2.2. Methods

Computational Simulations:

The primary tool for analysis was the COMSOL Multiphysics software, a powerful platform for simulating physical phenomena. The following steps outline the simulation process:

- a) **Modeling the Designs:** Detailed 3D models of both the trapezoidal and water drop designs were created using CAD software and imported into COMSOL. The geometric parameters for each design were carefully defined to match real-world specifications.
- b) **Defining Material Properties:** The material properties of aluminum and the absorptive coating were input into the software, ensuring accurate simulation results.
- c) **Setting Up Boundary Conditions:** Appropriate boundary conditions were established to simulate the environment accurately. This included defining the incident sound waves and the reflective properties of the materials. The simulations were conducted under standardized environmental conditions to maintain consistency.
- d) **Simulation Execution:** The STL for both designs was calculated across a range of frequencies (100 Hz to 5000 Hz). The simulations were run iteratively to verify the consistency and reliability of the results.

2.3. Analysis, Calculations, and Background

2.3.1. Acoustic-structure analysis

Domain equations:

In the realm of pressure acoustics, simulating harmonic sound waves, especially in aquatic environments, involves using the Helmholtz equation to model sound pressure dynamics [24];

$$\nabla \cdot \left(-\frac{1}{\rho_c} \nabla p \right) - \frac{\omega^2 p}{\rho_c \cdot c_c^2} = 0 \quad (1)$$

Here, p represents pressure (N/m²), ρ_c is the fluid's density (kg/m³), ω is the angular frequency (rad/s), and c_c is the speed of sound (m/s). Although both the density and speed of sound can be complex-valued to account for energy dissipation, in this model, they are considered real due to the absence of damping effects.

Boundary Conditions:

At the outer boundary of the air domain, an incident plane wave simulates an incoming sound wave, while a spherical wave, produced by the cylinder, propagates outward from the system. This is implemented using the spherical wave radiation boundary condition in the Pressure Acoustics, Frequency Domain interface. The incident wave's direction \mathbf{k} is defined by angles θ (0 to π) and ϕ (0 to 2π). Parameters for the incident wave are specified under the Incident Pressure Field feature.

Interface Cylinder-Water

The coupling between the fluid domain (pressure waves) and the solid is handled by the Acoustic-Structure Boundary multiphysics coupling. The boundary load F on the solid cylinder is given by [24];

$$F = -n_s p \quad (2)$$

where n_s is the outward-pointing unit normal vector in the solid domain. In equation 2, the unit of F is Newton, n_s is unitless quantity, and p is pressure in Pascal (Pa); however, since the pressure is associated with the load expressed in Newtons [N], the multiplication of the pressure by the unit normal vector yields a result in Newtons [N].

On the fluid side, the normal acceleration is matched with the solid's normal acceleration [24];

$$-n_a \cdot \left(-\frac{1}{\rho_0} \nabla p + q \right) = a_n \quad (3)$$

where n_a is the outward-pointing unit normal vector in the acoustics domain, and a_n is the normal acceleration of the solid, given by $(n_a u) \omega^2$, where u is the calculated harmonic-displacement vector of the solid structure.

Hard-wall comparison

For comparison, a simplified model treats the solid boundary as an impenetrable barrier, unaffected by acoustic waves but influencing the sound distribution. This is modeled by fixing displacement (u) to zero, resulting in the sound hard boundary condition [24];

$$n_a \cdot \left(-\frac{1}{\rho_0} \nabla p + q \right) = 0 \quad (4)$$

2.3.2. Sound transmission loss analysis

A key measure for evaluating a material's effectiveness in sound insulation is the STL, also referred to as the sound reduction index. While the specifics of its computation will be elaborated upon in subsequent sections, fundamentally, STL quantifies the disparity between incident and transmitted sound pressures. The STL value for a barrier is influenced by its material composition and structural design, varying across different frequencies. The primary determinant of STL across a spectrum lies in the frequency-specific response, which allows for the categorization of the STL profile into four distinct frequency-based regions, as depicted in Figure 3, as outlined in the sections that follow.

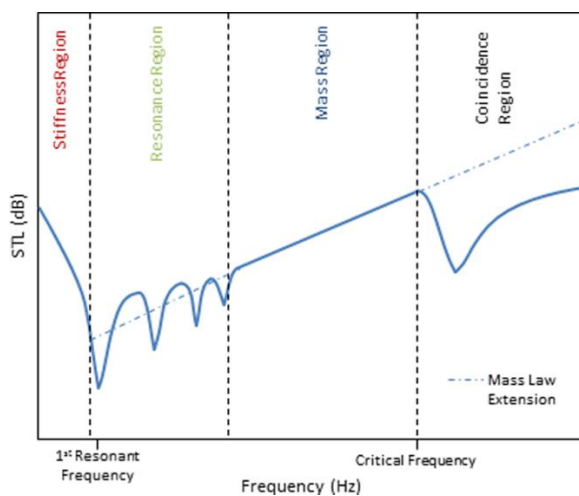


Figure 3. Frequency-dependent sound transmission regions of a panel [30].

In the lower frequency spectrum, the stiffness of the panel primarily dictates the STL, with damping and mass playing minimal roles, as seen Figure 3. Within this bandwidth, an increase in STL is noted alongside an elevation in the panel's first resonance frequency, culminating at the onset of this resonance. As frequencies ascend slightly above this threshold, the panel's natural resonances take precedence in influencing STL. These resonances, indicative of heightened panel vibrations, are determined by the panel's material, dimensions, and installation specifics. The interaction with these resonant frequencies results in significant sound energy transfer across the panel, manifesting as marked reductions in STL [30].

Progressing beyond the resonance domain, the panel's STL enters the mass-controlled region, which is crucial for numerous sound insulation endeavors. It is in this domain that the mass law comes into play, offering a precise STL estimation based on the panel's mass [30].

$$STL = 10 \log \left[1 + \left(\frac{m\omega \cos \theta}{2\rho c} \right)^2 \right] \tag{5}$$

Where m denotes the mass per unit area, ω signifies the angular frequency, θ is the incident angle, ρ represents the density of the acoustic medium, and c is the velocity of sound within the acoustic medium. For waves that are normally incident, the angle of incidence is 0° . By substituting this angle into the equation, converting the angular frequency to cyclic frequency (where $\omega/2\pi=f$), and assuming that $m\omega/(2\rho c)\gg 1$, the mass law can be simplified to the normal incidence mass law [30];

$$STL = 20 \log(fm) - 42 \text{ dB} \tag{6}$$

where f is the cyclic frequency in Hertz and m is the mass per unit area. While Eq. 6 is an empirical law, it accurately describes sound transmission in the mass region and provides a rough estimate for sound transmission in the resonance region. At even higher frequencies, bending waves can cause the phenomenon known as the coincidence effect. The coincidence effect first appears at the critical frequency (f_c) of the panel, which is given by [30];

$$f_c = \frac{c^2}{1.8h} \sqrt{\frac{\rho}{E}} \tag{7}$$

In this formula, c represents the speed of sound within the material, ρ denotes the material's density, and E signifies the material's elastic modulus. The coincidence effect emerges when the wavelengths of the bending waves within the barrier align with those of the incoming sound waves. Such alignment ensures that the bending movement of the barrier synchronizes with the surface movements of the panel. This synchronization facilitates a heightened transfer of sound energy from the incident waves to the other side of the panel, leading to a significant reduction in STL, a phenomenon often described as the coincidence dip, commencing at the critical frequency. This specific frequency range is identified as the coincidence region.

The STL through a building component, like a door, a window, a wall segment, or a sound insulation structure, is defined as the ratio expressed in dB of the total incident power P_{in} on the structure relative to the total transmitted power P_{tr} [25];

$$STL = 10 \log_{10} \left(\frac{P_{in}}{P_{tr}} \right) \tag{8}$$

STL measurements are calibrated under the assumption of a diffuse acoustic environment on the source side. There are established standards for STL assessment, such as ASTM E90 and ISO 10140, all designed to either directly or indirectly quantify the power of both incident and transmitted sound waves. A prevalent methodology employed is known as the two-room technique. This approach typically involves a reverberation chamber on the source end. Depending on the setup, the receiving end may also feature a

reverberation room (creating a reverberant-reverberant configuration) or, alternatively, an anechoic chamber (resulting in a reverberant-anechoic setup). Illustrations of these setups are provided in Figure 4 for visual reference.

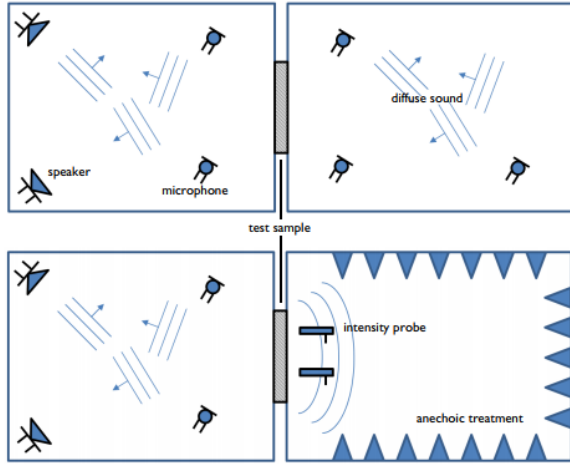


Figure 4. Two variations of the two-room configuration for measuring the sound transmission loss. Top: source and receiver reverberation rooms. Bottom: source reverberation room and receiver anechoic room [25].

In both cases, the incident power on the source side is computed as [25];

$$P_{in} = \frac{p_{rms}^2}{4\rho_0 c_0} S_s \tag{9}$$

where S_s is the area of the test surface on the source side (the area of the concrete wall tested), p_{rms} is the RMS pressure in the source room, ρ_0 is the air density, and c_0 is the speed of sound in air. This expression is derived by considering the incident power on a surface in an ideal diffuse acoustic field.

The expressions used to compute the incident and transmitted power for the reverberant case are only valid as long as the acoustic field is diffuse. A measure for the upper limit of modal behavior is given by the Schroeder frequency [25];

$$f_s = 2000 \sqrt{\frac{T_{60}}{V}} \tag{10}$$

where V is the room volume and T_{60} is the reverberation time. A room of volume V is said to be acoustically large when the studied frequency f is larger than the Schroeder frequency, giving the condition [25];

$$V > \left(\frac{2000}{f}\right)^2 T_{60} \tag{11}$$

Reverberant-Reverberant Setup

In the setup where the receiver room is a reverberation room (Figure 4 top) and the sound field is assumed to diffuse, the transmitted power is given by [25];

$$P_{tr} = \frac{p_{rms}^2}{4\rho_0 c_0} A_r \quad A_r = \sum_i S_i a_i \tag{12}$$

where p_{rms} is the RMS pressure in the receiver room and A_r is the receiver room absorption area, that is, the sum of products between each surface area S_i and its absorption coefficient a_i . The expression stems from an energy balance consideration where the total absorbed energy is equal to the radiated energy of the source. Combining Equation 9 and Equation 12 gives the expression for the STL for the reverberant-reverberant setup [25];

$$STL = SPL_s - SPL_r + 10 \log_{10} \left(\frac{S_s}{A_r}\right) \tag{13}$$

where SPL_s and SPL_r are the average sound pressure levels in the source and the receiver room, respectively. Averaging is done on the squared pressure before transforming to the dB scale.

Note that a correction to Equation 12 is sometimes introduced based on the Waterhouse expression. In a room with a diffuse field, the RMS pressure at the walls will be larger by a factor of 2 because each incident wave is coherent with its corresponding reflected wave. The corrected expression reads [25];

$$P_{tr} = \frac{\rho_{(rms)}^2}{\rho_0 c_0^2} V_r \left(1 + \frac{s_r \lambda}{8V_r}\right) \frac{13.8}{EDT} \tag{14}$$

where EDT is the early decay time, V_r is the receiver room volume, S_r the receiver room surface area, and λ is the wavelength.

Reverberant-Anechoic Setup

In the reverberant-anechoic configuration (Figure 4 bottom), the transmitted power is directly measured on the receiver side using an intensity probe. The measurement is performed in several locations in front of the test element and averaged. The transmitted power is then simply given by [25];

$$P_{tr} = S_r I_{tr} \tag{15}$$

combining this expression with Equations 8 and 9 gives [25];

$$STL = SPL_s - SIL_{tr} + 10 \log_{10} \left(\frac{S_s}{S_r}\right) - 6.14 \tag{16}$$

SIL_{tr} is the transmitted sound intensity level, and for flat samples, $S_s = S_r$. The numeric constant stems directly from the definitions of SPL and SIL and the equations for the power, it is expressed as [25];

$$10 \log_{10} \left(\frac{1}{4} \frac{(p_{ref})^2}{I_{ref} \rho_0 c_0} \right) \approx -6.14 \quad (17)$$

where $p_{ref} = 20 \mu\text{Pa}$, $I_{ref} = 10-12 \text{ W/m}^2$, $\rho_0 = 1.2 \text{ kg/m}^3$, and $c_0 = 343 \text{ m/s}$.

When simulating the **STL**, it is preferable to avoid modeling the source and receiver rooms, as this would be computationally extremely expensive. Instead, the setup is based on assuming an ideal diffuse field on the source side and an ideal anechoic termination on the receiver side of the test sample. The model also assumes that the test sample has little influence on the sound field on the source side. This is true for relatively stiff structures with low acoustic absorption properties. This is the case for the concrete wall studied in this example. The sound field on the source side can then be defined as a sum of $2N$ uncorrelated plane waves moving in random directions. It can also be assumed that one-half of these waves travel in the negative x direction and the other half in the positive x direction. Knowing that the concrete wall is located in the $x = 0$ plane, only the waves traveling in the positive x direction contribute to the incident pressure on the wall surface. The source room pressure field traveling in the positive x direction is then [25];

$$p_{x,room} = \frac{A}{\sqrt{2N}} \sum_{n=1}^N \exp(-i(k_{n,x} x + k_{n,y} y + k_{n,z} z)) \exp(i \cdot \Phi_n) \quad (18)$$

$$\left. \begin{aligned} k_{n,x} &= \cos(\theta_n) \\ k_{n,y} &= \sin(\theta_n) \cos(\varphi_n) \\ k_{n,z} &= \sin(\theta_n) \sin(\varphi_n) \end{aligned} \right\} \quad (19a, b, c)$$

where the polar angles $0 \leq \theta_n \leq \pi/2$ and $0 \leq \varphi_n \leq 2\pi$ as well as the phase $0 \leq \Phi_n \leq 2\pi$ are independent random numbers and A is the amplitude of the plane waves; Φ_n and Φ_n are taken directly from uniform distributions, whereas θ_n is obtained as $\theta_n = \alpha \cos(\theta_n)$, θ_n being a random variable with a uniform distribution between 0 and 1. This ensures a uniform distribution of wave numbers over the desired hemisphere. In the model, a new set of random numbers is generated for each n in the sum. The term ensures that the field has a constant intensity for any choice of N . Because the plane waves are uncorrelated, the total mean square pressure in the source room is $prms_2 = 2px,room/2/2$, with the term $2px,room$ accounting for the total diffuse field (positive and negative x directions). The theoretical limit for

large N of the mean square pressure in the room (away from walls) is $prms,th2 = |A|/2$.

The concrete wall is located at $x = 0$, where the incident diffuse field is reflected. The reflected component of the field is [25];

$$p_{refl} = \frac{A}{\sqrt{2N}} \sum_{n=1}^N \exp(-i(-k_{n,x} x + k_{n,y} y + k_{n,z} z)) \exp(i \cdot \Phi_n) \quad (20)$$

The reflected field is coherent with the incident field, as discussed in Equation 12. At the surface of the concrete wall, the total pressure load applied to the structure is the sum of the incident and reflected pressures [25].

$$p_{wall} = p_{x,room} + p_{(refl)} \quad (21)$$

III. DISCUSSION of the RESULTS

Using COMSOL Multiphysics software, a comprehensive comparative analysis of trapezoidal and droplet (water drop) models is conducted to evaluate their performance in STL and sound propagation mitigation. Simulations were carried out across a broad frequency range in randomized noise environments, providing extensive data for both models.

The findings of the current study consistently demonstrated that the water drop design surpasses the trapezoidal model in sound transmission loss across various frequency bands. These results were validated against test data for the trapezoidal model, establishing a baseline for comparison. Subsequent analyses of the water drop design were aimed at achieving realistic mirroring.

The drawings and mesh views of both models, depicted in Figure 5 and Figure 6, provide detailed visual representations that support the comparative analysis and highlight the structural differences contributing to their sound insulation performance. A detailed overview of the results can be seen in Figures A1 and A2 in the appendices.

As depicted in Figure 7, this investigation highlights the water drop design's superior effectiveness in sound insulation. This conclusion was further validated against certified test results conducted on the panel, ensuring the accuracy and reliability of our computational predictions. The term "Iterative refinement" refers to the step-by-step review and optimization of simulation parameters. In this process, the results obtained in each simulation cycle were analyzed, parameters were adjusted as needed, and the simulation was then repeated. Through these improvement cycles, the accuracy of the model was enhanced, and the reliability of the results was ensured. Thus, the validity and consistency of the study's findings were strengthened.

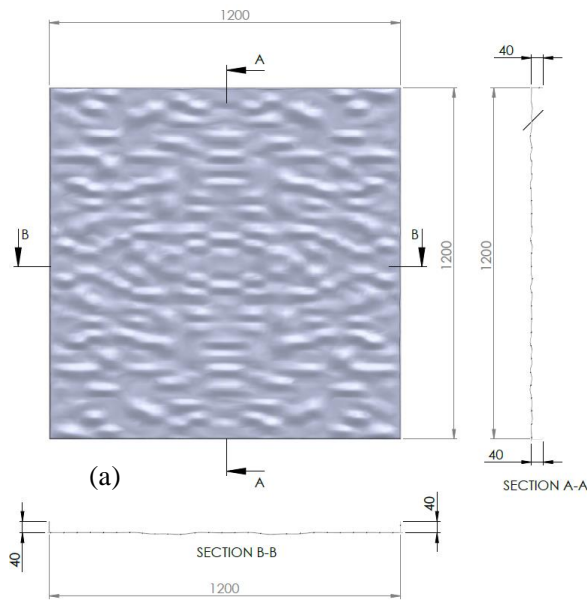


Figure 5. Drawing view of simulation sound barriers, (a) Water drop, (b) Trapezoidal.

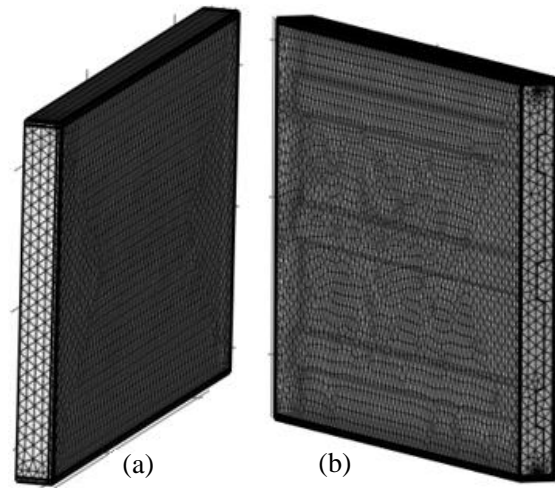


Figure 6. Meshing view of simulation parts. (a) Water drop, (b) Trapezoidal.

Figure 7 Compares the analysis results of the water drop and trapezoidal designs with the experimental results of the trapezoidal design. The figure clearly shows that the experimental and analysis data are closely aligned, substantiating the computational model's precision. This close correlation indicates that the superior performance of the water drop design observed in the analysis is likely to be replicated in real-world applications. Given this alignment, it can be confidently stated that the superior performance of the water drop design observed in the simulations is indicative of its likely superior performance in real-world conditions as well.

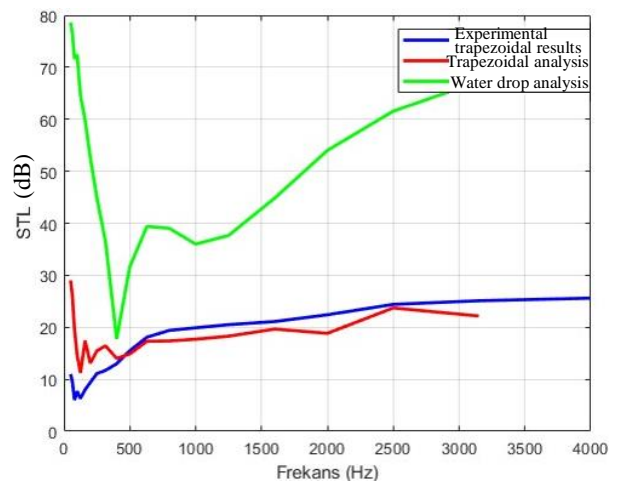


Figure 7. Comparison of analysis results of water drop and trapezoidal design with experimental results of trapezoidal design.

This study demonstrates that the same methodology can be employed to evaluate any desired design. By using advanced simulation tools like COMSOL Multiphysics, one can reliably predict the performance of various sound insulation designs, thereby facilitating informed decisions in the development of new noise

barrier systems. The versatility of this approach means it can be adapted to assess different geometric configurations and materials, making it a robust tool for sound insulation research.

3.1. Limitations and Considerations

Due to the lack of sufficiently competent software for comprehensive sound barrier analysis, the current study focused on evaluating the surface geometry of the designs rather than the entire structure. It is assumed the same absorbing materials between surfaces to reduce computational load and concentrate on the impact of surface geometry. This approach allowed us to isolate and analyze the effect of design geometry on sound insulation performance without the added complexity of varying material properties.

Specifically, the analysis was limited to surface geometry because current software solutions do not fully support comprehensive simulations of complete sound barrier systems. By maintaining consistent absorbing materials between surfaces, the analysis was simplified, allowing for a focused examination of geometric influences on sound insulation. This methodological choice helped to manage computational intensity and streamline the evaluation process.

The water drop design not only outperforms in sound insulation but also boosts aesthetic superiority, offering a visually striking appearance that enhances architectural and urban design.

Embracing innovative designs like the water drop model can enhance functionality in architectural solutions. This study underscores the need for a holistic approach that balances functional and aesthetic considerations in developing sound-insulating materials and systems.

3.2. Overall Comparison

The comparative analysis favors the water drop design over the trapezoidal model in both sound insulation effectiveness and aesthetic appeal. While the trapezoidal model has practical advantages, such as ease of production [25, 26], the water drop design offers superior performance in mitigating sound propagation and adds visual sophistication to architectural and urban design [27, 28]. Balancing functionality and aesthetics is crucial in developing sound-insulating materials and systems to enhance urban living standards [28, 29]. In conclusion, this study highlights the advancements in sound insulation technology and the importance of aesthetics in design decisions [13, 30]. The water drop design's superior performance in mitigating sound propagation, combined with its visual sophistication, makes it a valuable solution for enhancing urban living standards [31]. By embracing innovative designs like the water drop model, industries can achieve a balance between functionality and visual harmony, ultimately enhancing urban environments.

The fundamental physical principles used in the water drop design have been modeled with the same boundary conditions and material properties as in the trapezoid design. This supports that the results will have similar accuracy. The simulations of the water drop design were carried out using the same numerical methods and solution techniques employed for the Trapezoid design. Since the stability and accuracy of these methods have been previously validated, similar results are expected.

IV. CONCLUSIONS

This study has demonstrated the superiority of the water drop design over the trapezoidal model in both sound insulation effectiveness and aesthetic appeal. While the trapezoidal model offers practical advantages such as ease of production, the water drop design excels in mitigating sound propagation and adds visual sophistication to architectural and urban design.

The comparative analysis using COMSOL Multiphysics software, conducted over a wide frequency range in random noise environments, revealed that the water drop design consistently outperforms the trapezoidal model in terms of STL across various frequency bands. These findings were confirmed through simulations and verified test results, highlighting the water drop design's potential to enhance urban living standards by improving the quality of life in urban environments.

Furthermore, the study emphasizes the importance of balancing functionality and aesthetics in the development of sound-insulating materials and systems. The water drop design's ability to effectively mitigate sound propagation and its visually striking appearance make it an attractive solution for architects, urban planners, and policymakers. The results underscore the need for a holistic approach to urban planning and design that considers the interplay between sound insulation, aesthetics, and functionality. By embracing innovative designs like the water drop model, industries can create more livable and sustainable urban environments that prioritize the well-being of citizens.

REFERENCES

- [1] Moser, M. (2004). *Engineering Acoustics: An Introduction to Noise Control*. Berlin, Germany: Springer Science.
- [2] Raichel, D. R. (2006). *The Science and Applications of Acoustics* (2nd ed.). New York, USA: Springer Science.
- [3] May, D. N., & Osman, N. M. (1980). Highway noise barriers: New shapes. *Journal of Sound and Vibration*, 71(1), 73-101.
- [4] Ekici, I., & Bougdah, H. (2003). A review of research on environmental noise barriers. *Journal of Environmental Engineering*, 129(12), 1065-1073.

- [5] Degischer, H.-P., & Kriszt, B. (Eds.). (2002). *Handbook of Cellular Materials: Production, Processing, Applications*. Weinheim, Germany: WILEY-VCH.
- [6] Le, C. H. (2010). *Developments in topology and shape optimization*. Ph.D. Thesis, University of Illinois at Urbana-Champaign.
- [7] Eschenauer, H. (Ed.). (2006). *IUTAM Symposium on Topological Design Optimization of Structures, Machines and Materials*. Dordrecht, Netherlands: Springer.
- [8] Joshi, H. R. (2013). *Finite Element Analysis of Effective Mechanical Properties, Vibration, and Acoustic Performance of Auxetic Chiral Core Sandwich Structures*. M.Sc. Thesis, Purdue University.
- [9] Ramnath, B. V., Alagarraja, K., & Elanchezian, C. (2019). Influence of fiber orientation on the mechanical properties of GFRP composites. *Materials Today: Proceedings*, 16, 859-864.
- [10] Sayahlatifi, S., Rahimi, G., & Bokaei, A. (2021). An investigation into the acoustic performance of sandwich structures with auxetic cores. *Journal of Sandwich Structures and Materials*, 23, 94-109.
- [11] Li, Y., Wang, F., Jia, S., Ma, X., & Zhang, Y. (2021). Influence of process parameters on the mechanical properties of fiber-reinforced polymers. *Fibers and Polymers*, 22, 1718-1726.
- [12] Florence, M., Jaswin, M. A., & Pandi, A. P. (2020). Investigation of the tensile properties of fiber-reinforced polymers. *Fibers and Polymers*, 21, 1152-1160.
- [13] Arunkumar, M. P., Pitchaimani, J., Gangadharan, K. V., & Babu, M. C. L. (2017). Dynamic analysis of sandwich structures with auxetic core. *Journal of Sandwich Structures and Materials*, 19, 26-42.
- [14] Griese, D., Summers, J. D., & Thompson, L. (2015). Structural health monitoring of sandwich composites using vibration analysis. *Journal of Vibration and Acoustics*, 137, 021011.
- [15] Reiter, P., Wehr, R., & Ziegelwanger, H. (2017). Simulation and measurement of noise barrier sound-reflection properties. *Applied Acoustics*, 121, 11-21.
- [16] Moore, J. A., & Lyon, R. H. (1991). Sound transmission loss characteristics of sandwich panel constructions. *Journal of the Acoustical Society of America*, 89(3), 1544-1552.
- [17] Halliwell, R. E., & Warnock, A. C. C. (1985). Sound transmission loss: Comparison of conventional techniques with sound intensity techniques. *The Journal of the Acoustical Society of America*, 77(6), 2094-2103.
- [18] Garai, M., & Guidorzi, P. (2015). Sound reflection measurements on noise barriers in critical conditions. *Applied Acoustics*, 98, 103-109.
- [19] Asdrubali, F., & Pispola, G. (2007). Properties of transparent sound-absorbing panels for use in noise barriers. *Journal of Sound and Vibration*, 302(4-5), 840-854.
- [20] Laxmi, V., Thakre, C., & Vijay, R. (2022). Evaluation of noise barriers based on geometries and materials: A review. *Environmental Science and Pollution Research*, 29(10), 1729-1745.
- [21] Xiong, W. 2010. *Applications of COMSOL Multiphysics Software to Heat Transfer Processes*, Master Thesis, Department of Industrial Management, Arcada University of Applied Sciences, Helsinki.
- [22] Song, Y., Wen, J., Tian, H., Lu, X., Li, Z., & Feng, L. (2020). Vibration and sound properties of metamaterial sandwich panels with periodically attached resonators: Simulation and experiment study. *Journal of Sound and Vibration*, 486, 115559.
- [23] Khrystoslavenko, O., & Grubliauskas, R. (2017). Simulation of room acoustics using COMSOL Multiphysics. In *Proceedings of the 20th Conference for Junior Researchers "Science – Future of Lithuania" Environmental Protection Engineering (Article No. aplinka.06)*. Vilnius, Lithuania: Vilnius Gediminas Technical University.
- [24] Acoustic-Structure Interaction, https://www.comsol.com/model/download/1182151/models.aco.acoustic_structure.pdf (Access date: 12.09.2024)
- [25] Herring Jensen, M. J. (2020). Modeling sound transmission loss through a concrete wall, https://www.comsol.com/model/download/1177511/models.aco.sound_transmission_loss_concrete.pdf. (Access date: 12.09.2024)
- [26] Saadeghvaziri, M. A., & Macbain, K. (1998). Sound barrier applications of recycled plastics. *Transportation Research Record: Journal of the Transportation Research Board*, 1626(1), 83-89.
- [27] Bolton, J. S., Shiau, N.-M., & Kang, Y. J. (1995). Sound transmission through multi-panel structures lined with elastic porous materials. *Journal of Sound and Vibration*, 191(3), 317-347.
- [28] Oh, Y. K., & Kim, H. G. (2023). A preliminary study on the measurement method for determining the absorption coefficient of sound barrier panels [방음판의 흡음률 측정방법 제안을 위한 기초 연구]. *The Journal of the Acoustical Society of Korea*, 42(2), 152-160.
- [29] Oh, Y. K. (2022). A study on the standard for determining airborne sound insulation performance of sound barrier panels [방음판의 음향투과손실 측정규격에 관한 연구]. *Journal of Architectural Acoustics*, 35(3), 123-135.
- [30] Wang, D., Xie, S., Feng, Z., Liu, X., & Li, Y. (2020). Investigating the effect of dimension parameters on sound transmission losses in Nomex honeycomb sandwich. *Applied Sciences*, 10(9), 3109.

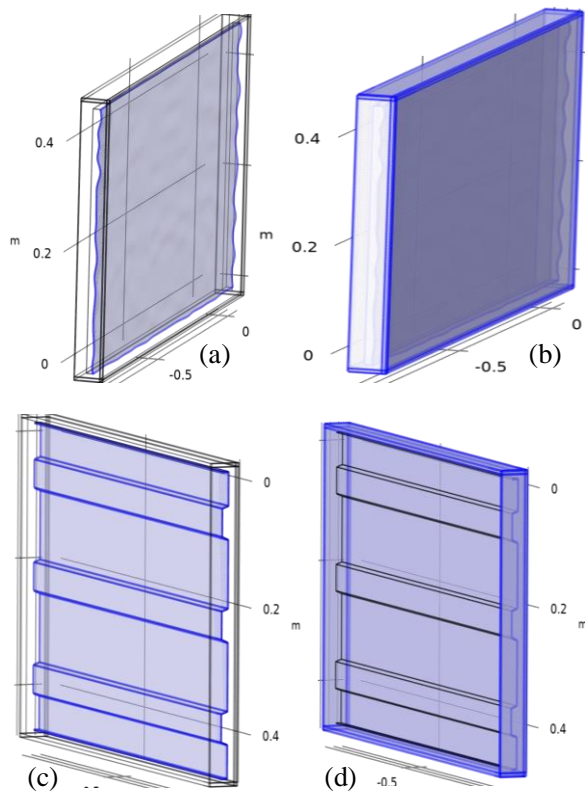
Appendices:

Figure A1. Some set up domain viewings, a) Water drop front face selection, b) Water drop back face selection, c) Trapezoidal front face selection, d) Trapezoidal back face selection.

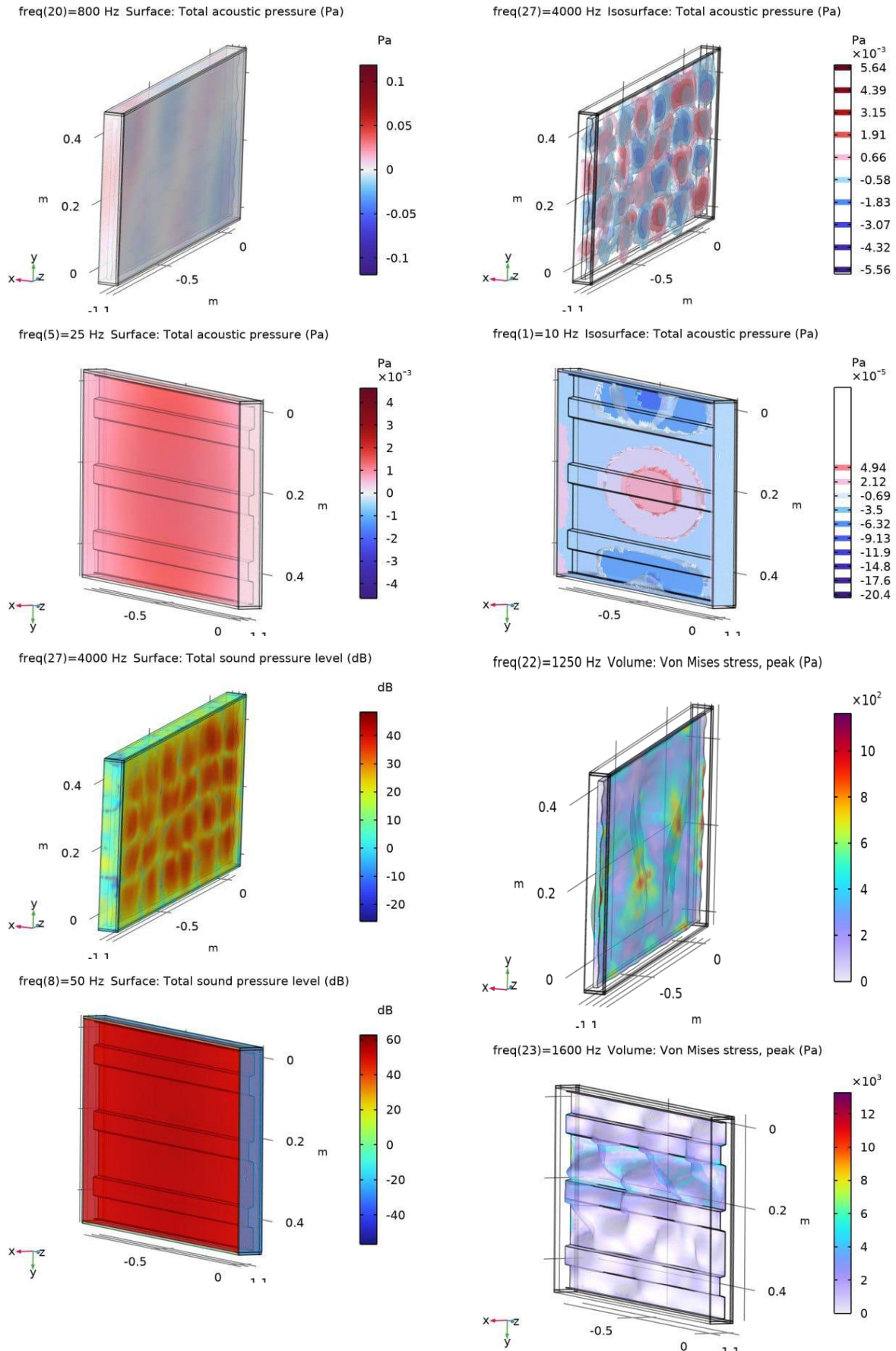


Figure A2. Some result viewings.